arXiv:2202.XXXXX

Homeostatic and Adaptive Energetics: Nonequilibrium Fluctuations Beyond Detailed Balance in Voltage-Gated Ion Channels

Mikhael T. Semaan* and James P. Crutchfield†
Complexity Sciences Center and Department of Physics and Astronomy, University of California, Davis, One Shields Avenue, Davis, CA 95616
(Dated: March 18, 2022)

Stochastic thermodynamics has largely succeeded in analyzing both equilibrium and arbitrarily far-from-equilibrium systems. It remains underapplied, however, in mesoscopic complex systems—particularly, biological ones—whose effective dynamics often violate detailed balance and whose microscopic degrees of freedom are often unknown or intractable, assumptions that stochastic thermodynamics commonly invokes. Using its tools, we review how to delineate *excess* and *housekeeping* energetics—the adaptive and homeostatic components of a system's thermodynamic behavior. Then, we extend stochastic thermodynamics with a trajectory class fluctuation theorem for nonequilibrium steady-state, nondetailed-balanced complex systems. Finally, we consider two neurobiological examples—voltage-gated sodium and potassium ion channels—to illustrate the results. These highlight the progress possible in understanding the thermodynamics of complex systems *without* restrictive assumptions and exhaustive knowledge of every underlying degree of freedom.

I. INTRODUCTION

Nonequilbrium phenomena pervade nature. In their many forms, energy gradients send hurricanes and wildfires to ravage, volcanoes to form and erupt, life to emerge. Mesoscopic complex systems—a planetary climate, forest ecosystems, the human body—consist of microscopic degrees of freedom that are inaccessible, intractable, or simply unknown. In point of fact, much of the human body's biochemistry relies essentially on out-of-equilibrium dynamics to function, adapt, and maintain homeostasis. From a theoretical perspective, mesoscopic complex systems are fertile ground for honing tools to analyze nonequilibrium processes.

To date, describing energetic fluxes in complex systems—developing a suitable mesoscopic nonequilibrium thermodynamics—remains an ongoing challenge. In point of fact, mathematics and physics difficulties continue to hinder developing a deeper understanding of how these systems operate. The following leverages and extends tools from stochastic thermodynamics and information theory to address these challenges. To demonstrate the techniques, it takes up two suitably complex, mesoscopic neurobiological systems.

A. Nonequilibrium Steady States

A system is typically called nonequilibrium in two distinct senses. The first, and most common, refers to nonequilibrium *processes*—say, induced by rapid environmental driving—wherein a system evolves through a series of transient configurations. When the environmental drive remains fixed, such a system remains out of equilibrium as it *relaxes* to some stationary distribution over its states, determined by the environmental parameters. If that stationary distribution corresponds to a thermodynamic equilibrium, we say the system possesses an *equilibrium steady state* (ESS), irrespective of its (perhaps highly nonequilibrium) driven, transient dynamics.

The second sense refers not to the transient behavior but to the nature of the stationary distributions: a *nonequilbrium steady state* (NESS) system is one whose steady states are themselves out of thermodynamic equilibrium. This is simply achieved by, for example, putting a system of interest in contact with two heat baths at different temperatures. Rayleigh-Bénard convection [1] exemplifies this phenomenon: the temperature gradient between the top and bottom boundaries ensures a constant flux of energy through the fluid, from the hotter to the cooler, *even when the gradient remains fixed indefinitely.* In this case it is not enough to identify the energetic fluxes due to the system's transient dynamics; we must also identify the energy required to maintain steady-state conditions in the first place.

NESSs appear even without multiple heat baths. For example, by optically dragging a bead through viscous fluid [2]—an experimental realization of the general case implied by nonconservative force-driven Langevin dynamics; by coarse-graining microstates [3]; or by contact with reservoirs of distinct electrochemical potentials—the case in virtually all common electrical circuits via Joule heating [4]. They emerge as well in the voltage-gated ion channels we consider.

A first attempt to give NESS systems a full thermodynamic framing defined the *housekeeping* heat Q_{hk} as the portion of the total heat Q that maintains NESS conditions [5]. (In this, the total energy is that exchanged between a system and its thermal environment, often idealized as a fixed-temperature bath.) What remains is

* msemaan@ucdavis.edu
† chaos@ucdavis.edu

the energy exchanged owing to the system's relaxation to steady state, termed the *excess* heat Q_{ex}:

$$Q = Q_{\text{ex}} + Q_{\text{hk}}. \tag{1}$$

Contrast this with an equilibrium system's steady states. Its ESSs, being in equilibrium, exchange no net energy with the thermal environment. In this setting, $Q_{\text{hk}} = 0$ and so *all* heat dissipation is excess: $Q_{\text{ex}} \to Q$. In other words, Q_{ex} in the NESS setting carries the same meaning as *total* heat Q in the ESS setting, and vice versa.

B. Approach

Equilibrium thermodynamics and equilibrium statistical mechanics prove insufficient to analyze nonequilibrium processes [6]. That said, recent advances in stochastic thermodynamics now successfully describe fluctuations in a variety of far-from-equilibrium systems. This has been done both in the first sense (relaxation to ESSs) [7–10] and in the second (NESSs) [11–13]. Reference [14] gives a recent review.

The following applies and extends these advances to analyze two complex neurobiological systems: voltage-gated sodium and potassium ion channels [15]—biophysical systems that originally motivated introducing master-equations for NESSs [16]. This elucidates, for the first time, their nonequilibrium behavior under the realistic, dynamic environmental drive of an action potential spike. In doing so, a toolkit emerges whose validity extends to a host of other mesoscopic complex systems—even those for which a purely energetic interpretation is impossible or problematic—provided a relatively small set of constraints on their effective dynamics holds.

Our development unfolds as follows. First, Sec. II lays out the relevant notation for our model classes and introduces appropriate *excess* thermodynamic functionals for describing them. Section II C, in particular, elaborates on the relationship between housekeeping heat, (ir)reversibility, and detailed balance. Section III A reviews *fluctuation theorems*—which bind nonequilibrium thermodynamic fluctuations to steady-state quantities. It closes in Sec. III C with our primary theoretical result: the first full trajectory class fluctuation theorem valid for NESS systems.

Moving to applications, Sec. IV introduces our example neurobiological systems: voltage-gated sodium and potassium ion channels embedded in neural membranes. Section V then applies the techniques developed in the preceding sections to the channels, illustrating and comparing their responses under realistic action potential spikes.

These results serve three roles. First, they show how the trajectory class fluctuation theorem evades the divergences implied by systems with one-way only transitions. Second, they quantitatively demonstrate how failing to account for housekeeping dissipation violates the appropriate fluctuation theorems, suggesting an important direction for experimental effort. Finally, despite marked differences between the ion channels' steady-states, the results show how to directly compare the channels' *excess* energetics. This both circumvents implied housekeeping divergences and allows for meaningful comparisons between their *adaptive* responses to the same environmental stimulus.

II. PRELIMINARIES

The central object here is the finite-length *controlled stochastic process* $X_{0:N} \doteq X_0 X_1 X_2 \ldots X_N$, where $X_i \in \mathcal{X}$ is the random variable corresponding to the state of a system under study (SUS) at times $\{t_i \in \mathbb{R} : i = 0, \ldots, N\}$. We call a specific realization $x_{0:N}$ a *trajectory*. The process's dynamics are not stationary; rather, they are driven by a *protocol* $\alpha_{0:N}$. Figure 1 illustrates the scheme.

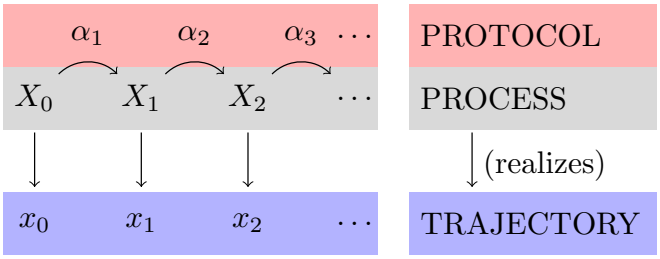

FIG. 1. Interaction between the stochastic process $X_{0:N}$, protocol $\alpha_{0:N}$, and realized (observed) trajectories $x_{0:N}$.

The following development places the following constraints on the SUS.

1. Each system parameter α_i leads to a stationary and ergodic stochastic process, realized by holding the protocol fixed indefinitely at α_i. This implies a unique would-be steady-state distribution $\boldsymbol{\pi}_{\alpha_i}$ associated to each α_i.
2. The state and protocol spaces are *even parity*, in the sense that we do not negate their values under time reversal, defined precisely later. Section II C discusses removing this assumption.

We emphasize these are *all* that is required for the main theoretical result and for meaningful definitions of the excess and housekeeping functionals. Importantly, we do not require dynamics of any particular form or possessing any particular structure—Markovian, Langevin, detailed balanced, Hamiltonian, master equation, coupled to ideal baths, and so on—beyond that specified by the two conditions above. We do not require states to be *microscopic*; they can correspond to arbitrary or unknown coarse grainings. With this in mind, even the discrete succession of events is flexible. In particular, from any

continuous-time dynamic we may generate a corresponding discrete-time one for appropriately small time steps.

While one cannot, in this most general setting, determine *energetics*, the fluctuation theorems introduced hold independently and exactly—and at any level of system description. We state the fluctuation theorems in this setting for two primary reasons: first, for clarity of derivation; second, with an eye toward future applications beyond thermodynamic systems to generally nonstationary stochastic processes.

A. The Thermodynamic System

That said, generality can hinder ease of application. To this end, when presenting the theoretical tools in their general forms, we frequently return to the relevant example—a "thermal system"—of Fig. 2. This is a SUS coupled to an ideal heat bath at inverse temperature $\beta = 1/k_{\mathrm{B}}T$, an ideal work reservoir parameterized by α, and an *auxiliary reservoir* representing the otherwise unaccounted-for degrees of freedom. Furthermore, we assign to each SUS state x an energy $E_\alpha(x)$. Finally, while the example system does not assume (order-1) Markov dynamics, it *does* assume no dynamical dependency on times before t_0. That is, the system's initial preparation is sufficient to determine the stochastic dynamics during the protocol.

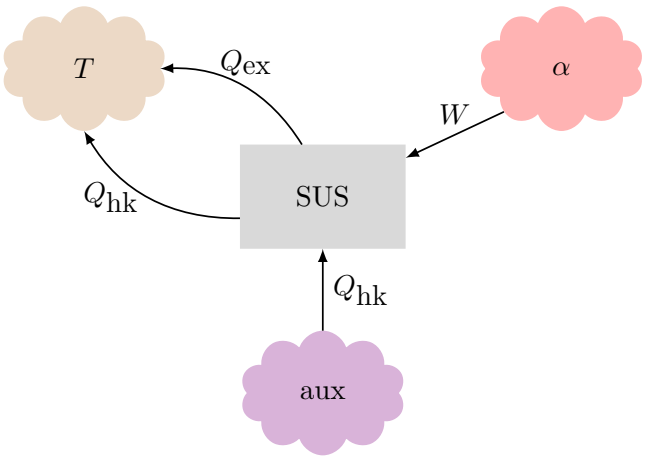

FIG. 2. A *thermal system* and its interactions with various baths. While heat and work reservoirs (labeled with temperature T and parameter α, respectively) are ideal, by design we assume nothing about the auxiliary or "aux" reservoir. The labels and arrow directions indicate energetic fluxes to-from the system. Notably, we allow for nonequilibrium steady states and functionally split the total heat Q into the *excess* heat Q_{ex}—corresponding to *adaptive* dissipation—and *housekeeping* heat Q_{hk}—referring to *homeostatic* dissipation.

The additional restrictions allow identifying the *energies* associated to each dynamical functional—introduced shortly. While they are the minimal possible constraints, they still allow the SUS to be coarse grained. And, this implies in general that the energetic fluxes are bounds rather than strict equalities [3].

Of paramount importance—and missing from most thermal system schemes—is the presence of the auxiliary bath. The heat and work reservoirs are each proxies for distinct *kinds* of coarse-grained degrees of freedom with distinct internal structures. The heat reservoir is an infinitely large source of purely thermal energy. The work reservoir is completely without entropy. Its only role is to set the SUS's energetic landscape via parameters α.

In contrast, there are no restrictions on the auxiliary reservoir's structure. It is unnecessary when describing the SUS's effective state (or energy) at any particular time. Partly, the auxiliary reservoir stands in for coarse-graining out unknown degrees of freedom by unknown schemes. Yet, the auxiliary reservoir's relevance goes beyond this. Specifically, Sec. II C shows that it is a *necessary* source for maintaining NESS conditions.

Altogether, the framework captures a large class of mesoscopic physical, chemical, biological, and engineered systems that exhibit nonequilibrium steady states, but that have additional structure and are in contact with a thermal environment. Subsequent sections develop tools for calculating all the associated energetic fluxes and for bounding their nonequilibrium fluctuations. Practically, this suggests experimental calorimetry and introduces a valuable way to *calibrate* effective models of, for example, the neurobiological ion channels we take up later.

B. Excess Energetics

With an ESS in contact with a single heat bath, the familiar First Law defines work and heat as distinct contributions to the ESS's energy change over the course of a protocol [8]:

$$\Delta E = \underbrace{\int \partial_\alpha E_\alpha(x)\, \mathrm{d}\alpha}_{\doteq\ W} + \underbrace{\int \partial_x E_\alpha(x)\, \mathrm{d}x}_{-\,Q.} \tag{2}$$

That is, W denotes a difference in system energy owing to a change in protocol—a change in the overall energy *landscape*—and Q denotes the difference owing to a change in system state—a dissipative signature of its *adaptation* to environmental conditions.

In contrast, the general setting may not provide a meaningful notion of energy. Worse, even in the restricted case of Fig. 2, we can no longer define total heat—as in Eq. (2)—for a NESS system. It leads to contradiction.

To see this, consider a fixed protocol at α and a system poised already in the distribution $\boldsymbol{\pi}_\alpha$. By definition then $W = 0$ and so $\langle W \rangle = 0$, where $\langle \cdot \rangle$ denotes a weighted average over all possible paths. We also have $\langle \Delta E \rangle =$

$\Delta \langle \boldsymbol{\pi}_\alpha | E_\alpha \rangle = 0$, where:

$$\langle \boldsymbol{\pi}_\alpha | E_\alpha \rangle \doteq \int_{x \in \mathcal{X}} \pi_\alpha(x) E_\alpha(x) . \tag{3}$$

Yet we cannot have $\langle Q \rangle = 0$, for by Eq. (1):

$$\begin{aligned} \langle Q \rangle &= \langle Q_{\text{hk}} \rangle \\ &\neq 0 \ , \end{aligned} \tag{4}$$

since this is a NESS system. In other words, when energy can flow at equal rates into and out of the system under study—as is the case for Q_{hk} from the auxiliary bath, through the system, and into the heat reservoir—that flux leaves no signature in the state energies.

However, there is an alternative to energy. Since to every parameter α is an associated steady-state distribution $\boldsymbol{\pi}_\alpha$, we can define the *steady-state surprisal*:

$$\phi_\alpha(x) \doteq -\ln \pi_\alpha(x) \ ; \tag{5}$$

so called as it is the Shannon self-information [17] of observing the system in state x under the distribution $\boldsymbol{\pi}_\alpha$.

Taking the surprisal's state average under this distribution yields its Shannon entropy (or, for continuous-state spaces, its differential entropy):

$$\begin{aligned} \langle \boldsymbol{\pi}_\alpha | \boldsymbol{\phi}_\alpha \rangle &\doteq \int_{x \in \mathcal{X}} \pi_\alpha(x) \phi_\alpha(x) \\ &= H[\boldsymbol{\pi}_\alpha] \ . \end{aligned} \tag{6}$$

To see how the surprisal relates to energy, consider the canonical ensemble of statistical mechanics—the ESS version of Fig. 2, with $Q_{\text{hk}} = 0$ and so no auxiliary bath—where $\boldsymbol{\pi}_\alpha$ is the Boltzmann distribution [18]. Then:

$$\begin{aligned} -\ln \pi_\alpha(x) &= \beta(E_\alpha(x) - F_\alpha^{\text{eq}}) \\ &= \phi_\alpha(x) \ , \end{aligned} \tag{7}$$

where F_α^{eq} is the equilibrium free energy—the familiar logarithm of the canonical partition function.

Equation (7) motivates yet another moniker for $\phi_\alpha(x)$: the *nonequilibrium potential*. In this sense, steady-state surprisal is analogous to a generalized energy. However, it remains a meaningful characterization of a system's steady-state distribution—via its information-theoretic interpretation—even when energy is not meaningful.

Leveraging this, an analogous First Law for $\phi_\alpha(x)$ defines the *excess* heat and work:

$$\begin{aligned} \Delta\phi = \underbrace{\int \partial_\alpha \phi_\alpha(x) \, \mathrm{d}\alpha}_{\doteq \ \mathcal{W}_{\text{ex}}} + \underbrace{\int \partial_x \phi_\alpha(x) \, \mathrm{d}x}_{-\mathcal{Q}_{\text{ex}}} . \end{aligned} \tag{8}$$

As with their nonexcess counterparts, these quantities characterize distinct *dynamical* contributions to a change in steady-state surprisal: $\mathcal{W}_{\text{ex}}$ capturing that due to a changing protocol, which sets the steady-state probability landscape; $\mathcal{Q}_{\text{ex}}$ monitoring a system's *adaptation* to its environment.

For Fig. 2's thermal system, these conveniently convert to energies: $\mathcal{W}_{\text{ex}} \to \beta W_{\text{ex}}$ and $\mathcal{Q}_{\text{ex}} \to \beta Q_{\text{ex}}$. And, they agree with other standard formulations of excess thermodynamic functionals [11, 13]. Using Eq. (7) and taking the ESS limit of Boltzmann-distributed steady-states yields: (i) $\mathcal{Q}_{\text{ex}} \to \beta Q$—with equilibrium steady states, all dissipated heat is excess—and (ii) $\mathcal{W}_{\text{ex}} \to \beta(W - \Delta F)$, leading to its classification as an *excess environmental entropy production* [13].

We stress, though, that the excess work and heat—and the steady-state surprisal—retain dynamical meaning independent of Boltzmann or even energetic assumptions. In this way, Eq. (7) is a guidepost for thermodynamic interpretation. It is not, however, a strict equivalence. In point of fact, as we will see, sodium channels (as with other NESS systems) lack a well-defined steady-state free energy [13]. Nevertheless, Eq. (8) describes—tractably—two functionally distinct aspects of their response to dynamic environments.

C. Detailed Balance and Housekeeping

The housekeeping heat remains. Recall that it corresponds to energy dissipated to maintain NESSs, as in Eq. (1). Phenomenologically, Eq. (1) provided a satisfactory answer. However, our excess heat definition only required would-be steady-state distributions exist. The definition of total heat, in contrast, depended explicitly on well-defined state energies. This difference led to problems with NESSs.

The upshot is that a more general definition of housekeeping heat is called for. In particular, it should depend only on the stochastic dynamics and, when added to excess heat, it should give a reasonable generalization of *total* heat. Naturally, we also require interpretability and that it reduces to the corresponding well-understood thermodynamic terms in the appropriate limits.

To these ends, but in a slightly more general form than previously reported, we define *housekeeping heat* to explicitly allow non-Markovian dynamics:

$$\begin{aligned} \mathcal{Q}_{\text{hk}} \doteq \ln & \frac{\Pr\left(X_{1:N} = x_{1:N} \mid X_0 = x_0; \alpha_{0:N}\right)}{\Pr\left(X_{1:N} = x_{N-1:0} \mid X_0 = x_N; \alpha_{N:0}\right)} \\ & + \ln \prod_{i=0}^{N-1} \frac{\pi_{\alpha_{i+1}}(\ x_i \ )}{\pi_{\alpha_{i+1}}(x_{i+1})} . \end{aligned} \tag{9}$$

Observe that the first term is a log-ratio of conditioned path probabilities. The denominator is the numerator's time reversal: the probability of obtaining the reversed path $x_{N:0}$ conditioned on starting in the state x_N and subject to the reversed protocol $\alpha_{N:0}$. The second term is exactly $-\mathcal{Q}_{\text{ex}}$ by the discrete form of Eq. (8). And so,

by identifying $\mathcal{Q} \doteq \mathcal{Q}_{\text{ex}} + \mathcal{Q}_{\text{hk}}$, housekeeping heat is a component of the generalized *total heat* $\mathcal{Q}$.

In the (single heat bath) thermal example, one recovers units of energy as $\mathcal{Q} \to \beta Q$ and $\mathcal{Q}_{\text{hk}} \to \beta Q_{\text{hk}}$. And, the resulting total heat is consistent with *microscopic reversibility* [9]. Equivalently, we could have started with this microscopic reversibility condition for even state spaces and arrived at the appropriate housekeeping heat.

With this in mind, consider *relaxing* the even state space assumption. Doing so and keeping the appropriate microscopic reversibility condition allows for an analogous splitting of housekeeping heat—modified so that the denominator's terms are negated where required—and excess heat, consistent with previous considerations of odd-parity NESS systems [19, 20]. While we note that an analogue to our Eq. (18) holds, we do not treat this further here.

Now, consider a Markov dynamic of order 1. That is, conditioning on the previous time step fully characterizes the probability distribution over futures. Then, the first term reduces to the logarithm of a product of one-step conditional probabilities. And, $\mathcal{Q}_{\text{hk}}$ tracks the degree of *detailed-balance violation* over the trajectory. This is in agreement with existing definitions [11, 13, 21]. Concretely, detailed-balanced dynamics imply $\mathcal{Q}_{\text{hk}} = 0$ for every trajectory. If any trajectory yields $\mathcal{Q}_{\text{hk}} \neq 0$, the dynamic is necessarily nondetailed balanced.

Finally, recall that by definition $\mathcal{Q}_{\text{hk}} = 0$ for an ESS system. Taken together with assuming an even state space—ensuring correct "reverse" probabilities—the Markov condition says, succinctly:

Nondetailed Balanced Dynamics

$\Updownarrow$

Nonequilibrium Steady States

Recall that the Markov condition is appropriate for many microscopically-modeled thermal systems such as overdamped Langevin dynamics, as well as for a host of biological systems like the ion channels we consider later.

Nonzero housekeeping heat actually *necessitates* including an auxiliary reservoir for a complete picture. Recall Fig. 2. This follows since a NESS system, even fully relaxed to its stationary distribution, constantly dissipates housekeeping heat to the thermal reservoir. (And does so at an average rate of $\mathrm{d}\left\langle Q_{\text{hk}}\right\rangle/\mathrm{d}t$.) Yet, with the protocol parameter fixed, no work (or excess work) is done: $W = 0$ by Eq. (2). The system's average energy does not change, though, since the parameter and individual state uniquely set its energies: $\mathrm{d}\left\langle E\right\rangle/\mathrm{d}t = 0$.

The conclusion is that energy flux through the system, observed in the housekeeping dissipation to the thermal reservoir, must come from *somewhere* not otherwise described by the ideal constructs. In other words, in the thermodynamically-interpretable setting, nondetailed balanced dynamics are signatures of unaccounted-for degrees of freedom. In this way, the constructions in Eqs. (8) and (9) provide the tools to isolate this *homeostatic* part of a system's energetic fluxes, so called for its role maintaining homeostatic (steady-state) conditions.

We close by calling out a feature on direct display in Eq. (9). While placing minimal restrictions on the *dynamics*, problems arise when any path is strictly irreversible, in the sense that a nonzero-probability forward trajectory is associated a zero-probability reverse. Then, $\mathcal{Q}_{\text{hk}}$ diverges. And this seemingly forbids dynamics in finite state spaces with one-way-only transitions.

In the thermodynamic interpretation, such a transition costs infinite dissipation. And, with this realization, usually a model's mesoscopic nature comes to bear. Indeed, Ref. [13] in its related sodium channel analysis remarks that "more careful experimental effort should be done to bound the actual housekeeping entropy production in these ion channels". The following section demonstrates that a new *trajectory-class fluctuation theorem* provides a tool for analyzing such experiments and circumvents the divergence while still placing strong bounds on fluctuations.

III. FLUCTUATIONS AND FREE ENERGY

So far, we defined the generalized quantities $\mathcal{W}_{\text{ex}}$, $\mathcal{Q}_{\text{ex}}$, and $\mathcal{Q}_{\text{hk}}$ and elucidated their meanings outside the ESS regime. As with their ESS counterparts, though, they depend on the specific path a system takes through its state space under a particular protocol. A suite of statistical tools called *fluctuation theorems* (FTs) tie such nonequilibrium behaviors to equilibrium (or steady-state, more generally) quantities. They come in three primary flavors: (i) *integral* FTs (IFTs) concern weighted averages over all possible trajectories; (ii) *detailed* FTs (DFTs) fix the relationship between a specific path and its associated reversal; and (iii) *trajectory class* FTs (TCFTs) interpolate between the two [22].

The following compares and contrasts these, discusses there role vis a vis free energy, and concludes with a trajectory-class FT for NESS systems. And, this then sets up analyzing two neurobiological NESS systems for their thermodynamic responses, expressed in excess works and housekeeping heats—to complex environmental signals.

A. Fluctuation Theorems

Integrated and detailed FTs each exhibit complementary tradeoffs—tradeoffs discussed below as we introduce the theorems. Trajectory-class FTs, meanwhile, combine the strengths of both and so are adaptable to a variety of systems and experimental conditions. Unlike the integral and detailed FTs, though, to our knowledge there is as yet no general trajectory-class FT valid for NESS systems. We address this lack by presenting one for the first

time. It simultaneously extends the previously-known ESS FT and reveals experimental difficulties unique to NESS systems, ultimately suggesting a need for new experimental tools.

Jarzynski's equality [7, 8], an IFT and the progenitor of the FTs we consider, links equilibrium free energies to the averaged exponential work distribution. It applies specifically to ESS systems that begin in their equilibrium distribution and are connected to a single heat bath. Under these conditions:

$$\left\langle \mathrm{e}^{-\beta W} \right\rangle = \mathrm{e}^{-\beta \Delta F} \ , \tag{10}$$

where the angle brackets refer to a weighted average over all possible trajectories. That is, Jarzynski's equality ties an arbitrarily nonequilibrium quantity—the averaged exponential work $\left\langle \mathrm{e}^{-\beta W} \right\rangle$—to the equilibrium free energy difference ΔF—a state function. Practically, this enables free energy estimation from nonequilibrium work measurements [23].

It comes with disadvantages, however. In particular, extremely rare paths often dominate the exponential work distribution [24], leading to poor statistical accuracy when estimating with finitely many experimental realizations. Nonetheless, Jarzynski's equality has been confirmed for a wide variety of systems [25–27]. In addition, while Eq. (10) only applies to ESS systems, a variety of generalizations have been derived and tested for NESS systems [2, 11, 12, 28].

In contrast to Jarzynski's IFT, the *detailed* FTs (DFTs), express a symmetry relation between a particular trajectory-protocol pair and its appropriate time reversal. Perhaps the most well-known of these is due to Crooks [9, 10], which is complementary to Jarzynski's IFT in several ways. For one, it makes the same assumptions: an ESS system connected to a bath, beginning in equilibrium and driven away from it. For another, Jarzynski's IFT results directly from trajectory-averaging both sides of Crooks' DFT. Before presenting the DFT, though, we pause to precisely define and set notation for what we mean by an "appropriate reversal".

Consider a system that begins in state distribution $\boldsymbol{\mu}_{\mathrm{F}}$, is driven by the protocol $\alpha_{1:N}$, and realizes a trajectory in the measurable subset $C \subseteq \mathcal{X}^{N+1}$. We call C a *trajectory class*. Then, we define the *forward process probability* as:

$$\mathcal{P}_{\boldsymbol{\mu}_{\mathrm{F}}}(C) \doteq \Pr\left(C \mid X_0 \sim \boldsymbol{\mu}_{\mathrm{F}}; \alpha_{1:N}\right) \ . \tag{11}$$

(Here, $\sim$ means "is distributed as".) Now, consider the same system beginning in the distribution $\boldsymbol{\mu}_{\mathrm{R}}$ and driven by the *reverse protocol* $\widetilde{\alpha}_{N:1}$, where the tilde indicates negation of time-odd variables (such as magnetic field). In turn, we define the *reverse process probability*:

$$\mathcal{R}_{\boldsymbol{\mu}_{\mathrm{R}}}(C) \doteq \Pr\left(C \mid X_0 \sim \boldsymbol{\mu}_{\mathrm{R}}; \widetilde{\alpha}_{N:1}\right). \tag{12}$$

For finite state spaces, Eqs. (11) and (12) define distinct probability measures on the trajectory space. In a continuous state space, we use the same notation to indicate probability *densities*.

Let $\boldsymbol{\pi}_{\mathrm{F}} \doteq \boldsymbol{\pi}_{\alpha_0}$ and $\boldsymbol{\pi}_{\mathrm{R}} \doteq \boldsymbol{\pi}_{\widetilde{\alpha}_N}$. In these terms, Crooks' DFT reads:

$$\frac{\mathcal{P}_{\boldsymbol{\pi}_{\mathrm{F}}}(x_{0:N})}{\mathcal{R}_{\boldsymbol{\pi}_{\mathrm{R}}}(\widetilde{x}_{N:0})} = \mathrm{e}^{\beta(W - \Delta F)}. \tag{13}$$

As for Jarzynski's IFT, the Crooks DFT has withstood experimental test [29] and seen use in empirically estimating free energy differences [23]. Also, paralleling Jarzynski's IFT, Crooks' DFT has been generalized to a variety of NESS systems [13, 30, 31].

We highlight Ref. [13]'s generalization of these. We recall, in particular, its Eq. (25), since it is the DFT upon which we base our TCFT.

Compared to Crooks' DFT, we assume an even state space. So, there is never negation under reversal. However, we do *not* assume equilibrium steady states (or detailed balance), any particular starting distribution for the forward and reverse processes, nor a single heat bath system (or any specific bath structure). Instead, we require only the functionals $\mathcal{W}_{\mathrm{ex}}$ and $\mathcal{Q}_{\mathrm{hk}}$ as defined in Eqs. (8) and (9), along with an additional one—the (unitless) *nonsteady-state free energy*:

$$\mathcal{F}^{\mathrm{nss}}_{\alpha}(\mu, x) \doteq \ln \frac{\mu(x)}{\pi_{\alpha}(x)} \ . \tag{14}$$

Its name derives from its indicating how far a given distribution is from the associated steady-state distribution. Indeed, on state averaging we have $\langle \boldsymbol{\mu} | \mathcal{F}^{\mathrm{nss}}_{\alpha} \rangle = D_{\mathrm{KL}}[\boldsymbol{\mu} \,||\, \boldsymbol{\pi}_{\alpha}]$. As with the other functionals generalized to the stochastic process picture, it carries meaning—departure from steady-state conditions—outside of energetic or thermal assumptions.

Given this, Ref. [13]'s DFT is:

$$\frac{\mathcal{R}_{\boldsymbol{\mu}_{\mathrm{R}}}(x_{N:0})}{\mathcal{P}_{\boldsymbol{\mu}_{\mathrm{F}}}(x_{0:N})} = \mathrm{e}^{-(\mathcal{W}_{\mathrm{ex}} + \mathcal{Q}_{\mathrm{hk}} - \Delta \mathcal{F}^{\mathrm{nss}})} \ , \tag{15}$$

where $\Delta \mathcal{F}^{\mathrm{nss}} = \mathcal{F}^{\mathrm{nss}}_{\alpha_N}(\boldsymbol{\mu}_{\mathrm{R}}, x_N) - \mathcal{F}^{\mathrm{nss}}_{\alpha_0}(\boldsymbol{\mu}_{\mathrm{F}}, x_0)$ is a correction due to starting the forward and reverse processes out of steady state. If we began the forward and reverse processes in their associated steady-state distributions, by definition we would have $\Delta \mathcal{F}^{\mathrm{nss}} = 0$.

As a mathematical statement involving a stochastic process' trajectories, their probabilities, and the functionals $\mathcal{W}_{\mathrm{ex}}$, $\mathcal{Q}_{\mathrm{hk}}$, and $\Delta \mathcal{F}^{\mathrm{nss}}$ we have so far defined, Eq. (15) holds *independent* of any thermodynamic assumptions. Yet, as before, reducing it to thermodynamically meaningful cases is straightforward and illuminates several important considerations when moving from ESS into NESS regimes.

B. Fluctuation Theorems and Free Energy

To see how the TCFT relates to other FTs, we apply Eq. (15) to Fig. 2's thermal system, since it represents the types of NESS system we wish to consider. Here, the change is to simply recover energy units:

$$\frac{\mathcal{R}_{\boldsymbol{\mu}_{\mathrm{R}}}\left(x_{N:0}\right)}{\mathcal{P}_{\boldsymbol{\mu}_{\mathrm{F}}}\left(x_{0:N}\right)} = \mathrm{e}^{-\beta(W_{\mathrm{ex}}+Q_{\mathrm{hk}}-k_{\mathrm{B}}T\Delta\mathcal{F}^{\mathrm{nss}})} \ . \tag{16}$$

In the ESS case, and starting in the associated steady states, Eq. (16) reduces directly to Crooks' DFT of Eq. (13). And so, from there, it reproduces Jarzynski's IFT via trajectory ensemble averaging.

Absent ESSs, though, there is no steady-state free energy term analogous to the equilibrium free energy. Rather, for ESSs: $W_{\mathrm{ex}} = W - \Delta F$. Generally, defining a NESS free energy is problematic [13], in part because steady-state distributions may no longer be Boltzmann. Instead, the excess work subsumes what would have been a change in steady-state free energy, and we work with it directly. The downside is the inability to extract a path-*independent* term from the path-dependent excess work.

Lacking our notion of excess work, Ref. [11] partially addressed this by writing $\Delta\phi + \mathcal{Q}_{\mathrm{ex}}$ directly—isolating $\Delta\phi$ as a path-independent quantity related only to initial and final configurations—and used this fact to derive a NESS Second Law from their IFT.

Mirroring this approach and adopting Fig. 2's assumptions, gives:

$$\frac{\mathcal{R}_{\boldsymbol{\mu}_{\mathrm{R}}}\left(x_{N:0}\right)}{\mathcal{P}_{\boldsymbol{\mu}_{\mathrm{F}}}\left(x_{0:N}\right)} = \mathrm{e}^{-(\beta Q+\Delta\phi-\Delta\mathcal{F}^{\mathrm{nss}})} \ . \tag{17}$$

This introduces yet another view of the problem with defining a NESS free energy. Since it contains the housekeeping heat, we cannot naïvely obtain W from Q, in terms of state energies. Instead, one way or another, this forces us to reckon with the path- and explicitly time-dependent housekeeping heat, either on its own or as part of the total heat. Still, Eq. (17)'s only path-dependence being in Q is an advantage, since it isolates a single thermodynamic variable in need of experimental tracking. It also brings to the forefront the primary challenge: In experiments, most often *work* is empirically tracked, even when testing a FT phrased in terms of heat [2].

C. NESS Trajectory Class Fluctuation Theorem

With an appropriate DFT for NESS systems now in hand, we are confronted with yet another challenging experimental tradeoff. Just as the IFTs suffer from extremely-rare extremely-large contributions, the DFTs require very precise control and measurement of *individual* realizations, as well as accurate estimations of individual realization probabilities (or their ratios). In many situations, this is intractable even in principle. For the ion channels considered shortly, generally *no* measurement of individual conformational states is available, since ion current is the only observable. Moreover, the state space topology varies with each individual rate model [32]. This is all to say that thermodynamic analysis requires a more flexible intermediary between the DFT's trajectory-level information and the IFT's ensemble-level information.

Reference [33] recently provided such an intermediary for ESS systems—the *trajectory class* FTs (TCFTs). At root, they relate the forward and reverse probabilities of an arbitrary subset of trajectories—the *trajectory class* C as introduced earlier—to the average exponential work *within* that trajectory class. In this way, TCFTs are maximally adaptable to experimental conditions: They need neither suffer rare event errors nor require individual-trajectory-level control. Instead, whatever the unique experimental conditions at hand, they provide a framework for laying out an associated FT. As a practical matter, TCFTs have already provided a diagnostic tool for monitoring the thermodynamics of successful and failed microscopic information processing in supercomputing flux logic [34].

The following extends Ref. [33]'s ESS TCFT (Eq. (3) there) in two ways. First, we allow for NESS systems. Second, we allow starting the forward and reverse processes in arbitrary distributions $\boldsymbol{\mu}_{\mathrm{F}}$ and $\boldsymbol{\mu}_{\mathrm{R}}$, respectively. The exponential NESS TCFT, derived in App. A, is:

$$\frac{\mathcal{R}_{\boldsymbol{\mu}_{\mathrm{R}}}\left(C_{\mathrm{R}}\right)}{\mathcal{P}_{\boldsymbol{\mu}_{\mathrm{F}}}\left(C\right)} = \left\langle \mathrm{e}^{-(\mathcal{W}_{\mathrm{ex}}+\mathcal{Q}_{\mathrm{hk}}-\Delta\mathcal{F}^{\mathrm{nss}})} \right\rangle_{C} \ , \tag{18}$$

where $\langle\cdot\rangle_C$ denotes the conditionally-weighted average over only those trajectories in the class C and the *reverse trajectory class* $C_{\mathrm{R}} \doteq \{\, x_{N:0} \,|\, x_{0:N} \in C \,\}$.

Equation (18) imports to the NESS setting all the benefits of the TCFT. Most notably, it adapts readily to a variety of experimental conditions while maintaining robust statistics. The associated DFT and IFT emerge simply by setting the class C to be a single trajectory or the set of all trajectories, respectively. Equation (18), as with its ESS counterpart, allows us to select the trajectories classes that are most accessible in a particular experimental configuration and *then* propose the appropriate theory against which to test.

Once again, in this form Eq. (18) makes only two assumptions about a stochastic process, as outlined previously: a unique stationary distribution for each α and an even state space. It reproduces Ref. [33]'s TCFT given ESS assumptions. Similarly, it reproduces Ref. [13]'s Eq. (52) when the class is chosen to start and end in a particular desired subset of states. However, our main result holds independently of any energetic, Markovian, or particular class assumption.

Generalization to NESS systems is not without caveat, however. $\mathcal{Q}_{\mathrm{hk}}$ plays a central role and we do not have

our state- and path-independent equilibrium free energy to extract from the average and estimate. This suggests experimentally tracking the housekeeping heat itself is key to understanding nondetailed balanced, NESS systems. (Alternatively, one could monitor the total heat per Eq. (17).) This is not surprising, considering Q_{hk} is *the* defining difference between an ESS and NESS system.

IV. Na^+ AND K^+ ION CHANNELS

Armed with this toolkit, we turn to two example systems: Ref. [15]'s delayed-rectifier potassium (K^+) and fast sodium (Na^+) voltage-gated ion channels. (See its Figs. 5.12 and 5.13, reproduced in our Figs. 3 and 4, respectively.) These single-channel models are based on relatively more macroscopic models of channel ensembles due to Hodgkin and Huxley [35]. However, they better represent the interdependencies between conformational transformations and more accurately reproduce experimentally-observed currents, especially for the Na^+ channel [15].

The models are both continuous-time Markov chains (CTMCs), whose dynamics are described by the stochastic master equation:

$$\frac{\mathrm{d}}{\mathrm{d}t}\,\langle \boldsymbol{\mu}(t)| = \langle \boldsymbol{\mu}(t)|\,\mathbf{G}_\alpha\,. \tag{19}$$

The row vector $\langle \boldsymbol{\mu}(t)|$ specifies the *state distribution* or *mixed state* at time t; its elements are $\mu(x,t) \doteq \Pr\left(X(t)=x\right)$. The transition rate matrix $\mathbf{G}_\alpha$ is controlled by the protocol and, thus, varies with time. The would-be steady-state distributions for each α are given by:

$$\langle \boldsymbol{\pi}_\alpha|\,\mathbf{G}_\alpha = \langle 0|\ , \tag{20}$$

with $\langle 0|$ the all-0 vector.

The transition-rate matrices corresponding to the two channels are:

$$\mathbf{G}_\alpha^{\mathrm{K}^+} = \begin{bmatrix} -4a_n & 4a_n & 0 & 0 & 0 \\ b_n & -(3a_n+b_n) & 3a_n & 0 & 0 \\ 0 & 2b_n & -(2a_n+2b_n) & 2a_n & 0 \\ 0 & 0 & 3b_n & -(3b_n+a_n) & a_n \\ 0 & 0 & 0 & 4b_n & -4b_n \end{bmatrix} \text{ and} \tag{21}$$

$$\mathbf{G}_\alpha^{\mathrm{Na}^+} = \begin{bmatrix} -3a_m & 3a_m & 0 & 0 & 0 \\ b_m & -(2a_m+b_m+k_1) & 2a_m & 0 & k_1 \\ 0 & 2b_m & -(a_m+2b_m+k_2) & a_m & k_2 \\ 0 & 0 & 3b_m & -(3b_m+k_3) & k_3 \\ 0 & 0 & a_h & 0 & -a_h \end{bmatrix}. \tag{22}$$

Letting α denote the transmembrane voltage, the associated transition rates are:

$$a_m(\alpha) = \frac{(\alpha+40\text{ mV})/10\text{ mV}}{1-\exp\left(-(\alpha+40\text{ mV})/10\text{ mV}\right)}, \qquad b_m(\alpha) = 4\exp\left(-(\alpha+65\text{ mV})/18\text{ mV}\right), \tag{23}$$

$$a_h(\alpha) = \frac{7}{100}\exp\left(-(\alpha+65\text{ mV})/20\text{ mV}\right), \qquad k_1 = \frac{6}{25}\text{ ms}^{-1},\ k_2 = \frac{2}{5}\text{ ms}^{-1},\ k_3 = \frac{3}{2}\text{ ms}^{-1}, \tag{24}$$

$$a_n(\alpha) = \frac{(\alpha+55\text{ mV})/100\text{ mV}}{1-\exp\left(-(\alpha+55\text{ mV})/10\text{ mV}\right)}, \text{ and} \qquad b_n(\alpha) = \frac{1}{8}\exp\left(-(\alpha+65\text{ mV})/80\text{ mV}\right). \tag{25}$$

We map these CTMC systems to discrete-time stochastic processes by taking $\alpha(t)$ fixed for sufficiently small time intervals Δt, generating the transition matrices:

$$\mathbf{T}_\alpha^{\Delta t} \doteq \mathrm{e}^{\Delta t\,\mathbf{G}_\alpha} \tag{26}$$

for each such time interval. Having discretized time in this way, they are examples of the thermodynamic scheme in Fig. 2, being surrounded by a single thermal environment at body temperature.

A voltage-gated ion channel's basic function is to selectively allow ions to permeate a cell membrane. The selection is based on the transmembrane voltage—the voltage difference between the membrane's inside and outside. In our models, this difference is specified by the parameter α, and so a neuronal action potential spike is a specific protocol. Reference [15]'s K^+ and Na^+ models correspond to channels that play crucial roles in generating and propagating such spikes in mammalian neurons. Both Markov chain models are estimated from single-channel experiments.

We selected these two channel models for several reasons. First, in terms of their biological function, they accomplish similar tasks, are connected to the same environ-

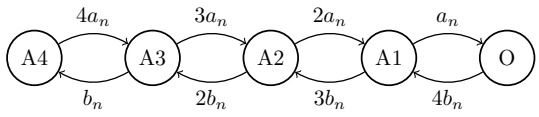

FIG. 3. Continuous-time Markov chain model of the K^+ channel adapted from Fig. 5.12 of Ref. [15]. Self-transitions are implied. In the states labeled An, n (between 1 and 4) activation gates close the channel. O labels the open channel state, the only one in which K^+ current can flow through the channel. The rate parameters a_n and b_n are voltage-dependent; their functional forms are given in Eqs. (25). This channel model is fully detailed balanced, in the sense that Eq. (27) is zero for every allowed transition pair.

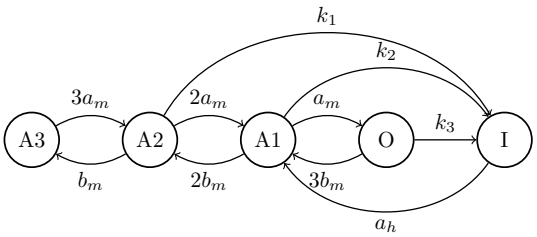

FIG. 4. Continuous-time Markov chain model of the Na^+ channel adapted from Fig. 5.13 of Ref. [15]. Self-transitions are implied. In the states labeled An, n (between 1 and 3) activation gates close the channel. O labels the open channel state, in which Na^+ current flows through the channel. Finally, I labels the channel's inactivation by its inactivation gate—its so-called ball and chain. The rate parameters a_m, b_m, and a_h are all voltage-dependent; their functional forms are given in Eqs. (23)–(24). The rate constants k_1, k_2, and k_3 are given by Eqs. (24). Unlike the K^+ channel, this model of the Na^+ channel features one-way transitions in the rate dynamic—states O to I and A2 to I. These transitions are maximally irreversible, and imply divergent infinitesimal housekeeping heat in the sense of Eq. (27). In addition to these, many of the other transition pairs do *not* satisfy detailed balance—Eq. (27) evaluates finite but nonzero.

mental parameters, and are suitably mesoscopic. That is, despite being more detailed than the Hodgkin-Huxley ensemble models, neither model accounts for the many additional degrees of freedom involved in the channel dynamics, be it steady-state or transient functions. The small effective state spaces in the Markov chain models reflect this.

One consequence of this implied coarse graining is that any total entropy production is a lower bound [3]. Still, we are able to make headway analyzing their nonequilibrium dynamics *without* knowledge of the underlying coarse-graining methods—knowledge missing for the vast majority of mesoscopic complex systems.

Second, the Na^+ channel's transition rates do not, in general, satisfy detailed balance, while the K^+ channel's do. Indeed, the Na^+ channel model includes both finitely nondetailed-balanced transition pairs and one-way-only transition rates, which imply divergent infinitesimal-time housekeeping heat.

To see this, note that under our time discretization and the Markov property, the *infinitesimal*(-time) *housekeeping heat* (a single "step" of Eq. (9)) for a transition between states indexed by i to j:

$$\begin{aligned}[\mathrm{d}\mathcal{Q}_{\mathrm{hk}}]_{ij} &= \lim_{\Delta t\to 0} \ln \frac{\pi_\alpha(x_i)\left[\mathbf{T}_\alpha^{\Delta t}\right]_{ij}}{\pi_\alpha(x_j)[\mathbf{T}_\alpha^{\Delta t}]_{ji}} \\ &= \lim_{\Delta t\to 0} \ln \frac{\pi_\alpha(x_i)[\mathbf{G}_\alpha + \mathcal{O}(\Delta t)]_{ij}}{\pi_\alpha(x_j)[\mathbf{G}_\alpha + \mathcal{O}(\Delta t)]_{ji}}. \end{aligned} \tag{27}$$

For systems with one-way-only transition rates, such as from the second to the fifth state of the Na^+ channel (indexing the states left to right, Fig. 4), infinitesimal housekeeping heat diverges. This contrast between the two channels—wherein one of them exhibits equilibrium steady states and the other nonequilbrium steady states—allows showcasing several features of the NESS TCFT and of the NESS framework more broadly.

As a test case, the K^+ channel should satisfy the ESS TCFT (where $\mathcal{Q}_{\mathrm{hk}} = 0$) while the Na^+ channel should violate it. Both, however, should satisfy our NESS TCFT of Eq. (18).

One benefit of the TCFT's averaging over arbitrary trajectory classes comes from avoiding the divergences implied by one-way transition rates: We select only those trajectories that do *not* include one-way transitions in the Na^+ channel, but still satisfy the appropriate DFT (and therefore TCFT) with those trajectories.

In this way, the NESS TCFT allows monitoring nonequilibrium fluctuations in systems with drastically different steady-state characteristics: detailed balance on the one hand and spurious divergences on the other.

Yet separating heat into excess and housekeeping components *also* enables direct comparison of the channels' *adaptive* energetics. Given the same environmental drive, which components of their dissipations are due solely to their internal adaptation to that drive? The excess heat, $\mathcal{Q}_{\mathrm{ex}}$. This remains true without regard for the divergence implied by one model's steady states. In essence, we cleave the housekeeping infinity to directly compare adaptive energetics.

Finally, both models are simple and illustrative. There are many more-detailed candidate state-space models for the Na^+ channel. Refer to, for example, those in Refs. [32, 36], whose variations have implications for understanding responses to drug treatments [37]. While we do not analyze them directly, our techniques generalize to

any such candidate models straightforwardly and provide an alternative formulation to that of Ref. [36]. Indeed, our ability to carry out these thermodynamic analyses provides new grounds for model selection, contingent on measurement techniques to experimentally extract the appropriate quantities.

V. METHODS AND RESULTS

Our goal, ultimately, is to describe the nonequilibrium thermodynamics of driven mesoscopic NESS systems. We take up the challenge here in two ways.

First, we numerically verify the NESS TCFT of Eq. (18), by sampling individual trajectories from both channels under the neurobiologically-plausible action potential *spike protocol*. We derived this protocol by solving the reduced ODEs (8.5) and (8.6) of Izhikevich [38] (also presented earlier [39]) with their Fig. 8.12's "regular spiking" parameters, integrating via the explicit forward Euler method. We start the transmembrane voltage at its resting potential (of -60 mV in this parameter set) and the recovery variable u at 0 and set the input DC current pulse at 70 pA. The ODEs simulate neuronal spiking and bursting based on macroscopic considerations. We take a single spike over a 200 ms protocol as our example.

Second, we calculate the full trajectory-averaged excess heat and work—$\langle \mathcal{Q}_{\text{ex}} \rangle$ and $\langle \mathcal{W}_{\text{ex}} \rangle$, respectively—of the two channel models under both a modified spike protocol and a *pulse protocol*, matching that of Ref. [13] and provided for comparison with their work. We modified the spike protocol—by setting the membrane capacitance to 1 pF and DC pulse of 80 pA—to change the time scale of a single spike from 200 ms to 2 ms, more accurately reflecting measurements in Ref. [15] and fast enough to showcase the different time scales of the channel model responses.

For both protocols, we take $1+10^5$ equidistant time steps. For the 12 ms pulse protocol, this gives 0.12 µs time steps. For the 200 ms and 20 ms spike protocols, it gives (respectively) 2 µs and 20 ns steps.

Admittedly, the selected ion channel models are not realistic in the sense that they do not incorporate feedback between the transmembrane potential and the ion channel states themselves. This feedback is crucial to *in vivo* generation of the spike patterns. Nonetheless, we argue this simplification is actually an *advantage* of our approach. We ask: *Given* a particular transmembrane protocol—regardless of how it got there—how do these individual channels respond? How do they absorb and dissipate energy in response to this environment?

A. Verifying the NESS TCFT

The primary results in this section compare the *detailed balanced* model of the K^+ channel with the nondetailed balanced one of the Na^+ channel, showing agreement between ESS and NESS FTs in the former but violation in the latter. The TCFT's flexibility effectively allows us to select only desired trajectories and take partial sums on either side of the underlying DFT. This not only helps gather experimental statistics, but also helps generate statistics from models, as we do here.

While Eq. (27)'s first-order approximation is valid in the infinitesimal time limit, *any* finite time step—no matter how small—maps every zero in the transition-rate matrices to nonzero values in the discrete-time transition matrices. As long as any state can transition to any other *eventually* in the rate dynamic, we observe a *direct* transition from any state to any other state after *any finite time*. Mathematically, this results from higher-order terms in the matrix exponentials. Problematically, this can induce nondetailed balance even in a detailed-balanced rate model, such as the K^+ channel, while at the same time removing the divergences due to one-way rate transitions in the Na^+ channel.

We resolve the issue for our purposes by explicitly considering the first-order approximation of Eq. (27). Formally, it defines a distinct discrete-time dynamic compared to taking the full matrix exponentials, but the fluctuation theorems apply just as well to this "approximated" dynamic. This also has the advantage of preserving detailed balance for the K^+ channel while implying divergent housekeeping transitions for the Na^+ channel. We avoid the divergent Na^+ transitions altogether by selecting only trajectories that do not include those transitions for consideration, yet another advantage the TCFT affords. This does not alter the TCFT's validity as long as we can collect the probabilities of the selected trajectories.

We can collect those probabilities, having the full transition dynamic in hand. However, simulating trajectories of length $N = 1 + 10^5$, the resulting probabilities are extraordinarily small. To ameliorate numerical precision issues, we collect the natural logarithm probabilities directly, conditional by conditional. Accordingly, we adjust the DFT kernel of Eq. (18):

$$\ln \frac{\mathcal{P}_{\boldsymbol{\mu}_{\text{F}}}(x_{0:N})}{\mathcal{R}_{\boldsymbol{\mu}_{\text{R}}}(x_{N:0})} = \mathcal{W}_{\text{ex}}[x_{0:N}] + \mathcal{Q}_{\text{hk}}[x_{0:N}] - \Delta\mathcal{F}^{\text{nss}} \ . \tag{28}$$

Since we wish to isolate the differences due to NESSs (or, equivalently in our case, to nondetailed-balanced dynamics), we make one final simplifying assumption before numerical simulation. We begin all forward and reverse processes in their local stationary distributions, effectively setting $\Delta\mathcal{F}^{\text{nss}} = 0$. This leaves us to directly verify:

$$\ln \frac{\mathcal{P}_{\boldsymbol{\mu}_{\text{F}}}(x_{0:N})}{\mathcal{R}_{\boldsymbol{\mu}_{\text{R}}}(x_{N:0})} = \mathcal{W}_{\text{ex}}[x_{0:N}] + \mathcal{Q}_{\text{hk}}[x_{0:N}] \ . \tag{29}$$

To test the NESS TCFT for both channels we plot the left hand side of Eq. (29) on the horizontal axis. On the

vertical axis, we plot both the full right hand side as well as the naïve partial excess work distribution that ignores housekeeping heat. The latter corresponds to the ESS TCFT of Ref. [33] and its underlying DFT due to Refs. [9, 10]. See Figs. 5 and 6.

Note that we labeled the RHS in units of $[k_{\mathrm{B}}T]$, being in contact with a single-temperature heat bath—a condition of Fig. 2 and an appropriate one for ion channels immersed in a single-temperature environment. In more general settings, the functionals $\mathcal{W}_{\mathrm{ex}}$ and $\mathcal{Q}_{\mathrm{ex}}$ are purely dynamical quantities, to be understood and interpreted as indicated in Secs. II B and II C.

While the various FTs hold regardless of the individual protocol used, we generated our comparisons according to the spike protocol for concreteness. We sampled trajectories according to their likelihood in the forward process, obtaining 1000 trajectories for the K^+ channel and 449 for the Na^+ channel.

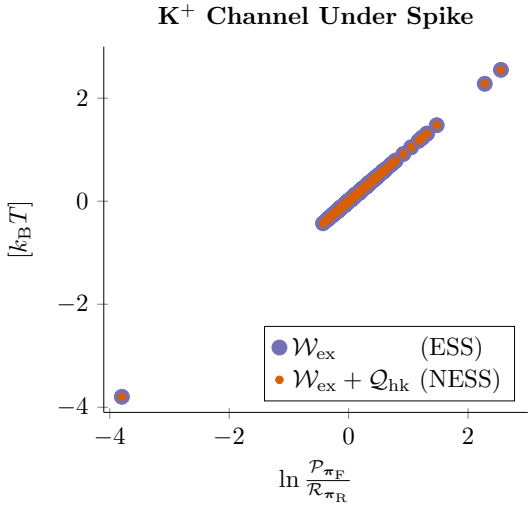

FIG. 5. K^+ channel driven by the spike protocol: Partial distributions of thermodynamic functionals with respect to the logarithmic reverse-forward trajectory probabilities. The blue and orange dots match exactly (one to one), indicating complete agreement between the ESS and NESS DFTs. This is to be expected since the K^+ channel is fully detailed balanced: $\mathcal{Q}_{\mathrm{hk}} = 0$ for each trajectory. That both sets of data points not only match but also lie on the identity confirms agreement with Eq. (28).

As expected, for the fully detailed balanced K^+ channel there is no disagreement between our and Ref. [33]'s primary TCFT, because $\mathcal{Q}_{\mathrm{hk}} = 0$ for every trajectory.

The Na^+ channel, in contrast, paints a different picture. Ignoring the nondetailed-balanced transition pairs in this trajectory class leads to rather strong violation of the NESS TCFT. This indicates disagreement between it and the ESS TCFT. Our Fig. 6 is roughly, but not exactly, analogous to Ref. [13]'s Fig. (6), but fleshes out a broader set of Crooks DFT violations. In fact, it reveals an interesting and surprising structure in the linear bands of violating-trajectory classes with slope less than unity.

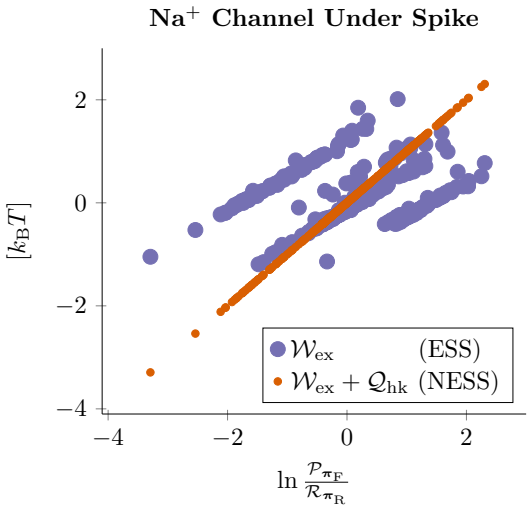

FIG. 6. Na^+ channel driven by the spike protocol: Partial distributions of thermodynamic functionals with respect to the logarithmic reverse-forward trajectory probabilities. That blue and orange dots do not agree one-to-one here indicates disagreement between the ESS and NESS DFTs. This is to be expected, since the Na^+ channel features several nondetailed balanced transition pairs, and so generic trajectories should have $\mathcal{Q}_{\mathrm{hk}} \neq 0$. The orange line confirms complete agreement with Eq. (28): the NESS DFT is satisfied. The scatter of blue dots showcases exactly how the same trajectories *violate* the ESS DFT—Crooks' FT, in this case. Interestingly, the violations possess their own nontrivial structure, with distinct bands of slope < 1 trajectories. Since each of these lines define their own trajectory class, this plot suggests further exploration of what else, if anything, distinguishes these classes.

On the one hand, our horizontal axis—the tunable parameter in the computational experiment—indicates the likelihood of a particular trajectory relative to its associated time reversal. A zero value here indicates reverse and forward processes with the same likelihood. Going right from 0, the *forward* process is increasingly more likely than its reverse. Going left from 0, the reverse process is increasingly more likely.

The vertical axis, on the other hand, corresponds to environmental entropy productions, since we begin and end in associated steady-state distributions. The orange dots represent the full environmental entropy production—excess plus housekeeping—while the blue represent ignoring the housekeeping term, which vanishes for an ESS system. Thus, the blue bands in Fig. 6 tell us that ignoring housekeeping *underestimates* how quickly entropy production grows with the forward path's relative likelihood.

The fact that there are distinct *bands* of these violations, however, augurs future fruitful explorations. Since each band itself defines a particular trajectory class, it will be interesting to investigate what—if anything—distinguishes these classes besides violating the Crooks DFT. Apparently, there are distinct mechanisms viola-

tion.

As a final consideration, we note that the ESS TCFT (and so the Crooks DFT) *do not claim* to be valid for NESS systems. That said, our results visually verify the facts that the NESS generalization both extends the range of validity of the TCFT and reduces in the correct way for ESS systems.

That we have a trajectory class form for the NESS TCFT, captured in our Eq. (18), imports its ESS progenitor's flexibility. That is, we need capture neither individual trajectory-level information to verify the DFT nor accurately sample the full trajectory space for an IFT.

Yet experimental verification remains a significant challenge. Generalizing to NESS systems requires not only the excess work distribution but housekeeping heats as well. Indeed, these results suggest that carefully considering how to measure housekeeping dissipation is crucial to characterizing fluctuations in NESS systems. As Fig. 6 demonstrates, improper accounting leads in general to TCFT *violations* and, if the ESS FTs are used to estimate free energy differences, to potentially drastically mischaracterizing the system of interest.

B. Average Excess Energetics

Despite the channels' seeming incompatibility revealed by the TCFT tests, we can compare the channels' adaptive energetics via the excess thermodynamics. We begin by directly calculating the full trajectory averages, obtaining for discrete time:

$$-\langle \mathcal{Q}_{\text{ex}} \rangle = \sum_{n=0}^{N-1} \langle \boldsymbol{\mu}(t_{n+1}) - \boldsymbol{\mu}(t_n) | \boldsymbol{\phi}_{\alpha_n} \rangle \text{ and} \tag{30}$$

$$\langle \mathcal{W}_{\text{ex}} \rangle = \sum_{n=0}^{N-1} \left\langle \boldsymbol{\mu}(t_n) \middle| \boldsymbol{\phi}_{\alpha_{n+1}} - \boldsymbol{\phi}_{\alpha_n} \right\rangle , \tag{31}$$

in agreement with Ref. [13]. As above, we set the initial distributions to the local stationary distribution for convenience. Armed with the discrete protocols, time steps, and starting distributions, we directly evaluate the mixed states (Eq. (19)) and steady-state distributions (Eq. (20)) for each time step. These are all that is needed to calculate $\langle \mathcal{Q}_{\text{ex}} \rangle$ and $\langle \mathcal{W}_{\text{ex}} \rangle$ via Eqs. (30) and (31).

Figures 7 and 8 give the simulation results for excess heat.

First, driven by the pulse protocol, the K^+ channel dissipates significantly more excess heat over the protocol's course. Its rate of relaxation to steady state—corresponding to constant epochs in the protocol—appears slower than the Na^+ channel's on the jump from -100 to 10 mV, but significantly faster on the subsequent drop back down to -100 mV.

The spike protocol paints a very different picture. Here, the Na^+ channel dissipates much more over the course

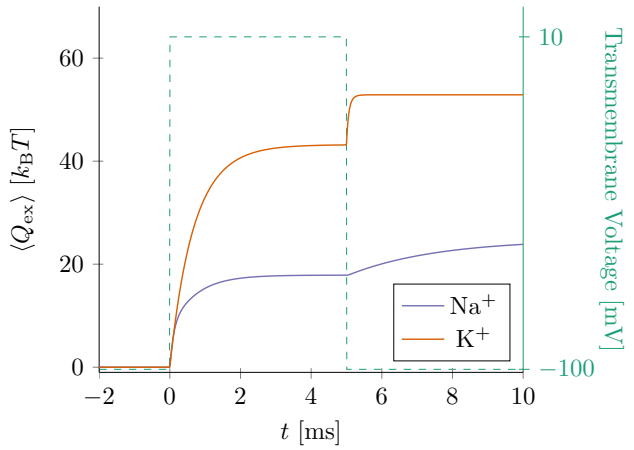

FIG. 7. Excess heats (solid lines) for both channels under the pulse protocol (dashed line). The K^+ channel is significantly more dissipative, illustrating the energy it expends as it relaxes to environmentally-induced steady state.

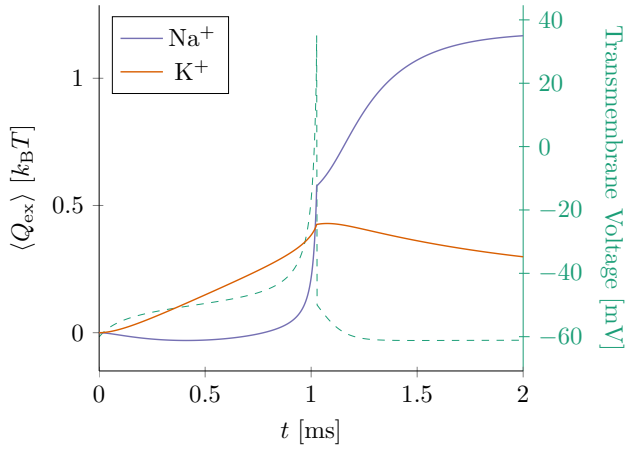

FIG. 8. Excess heats (solid lines) for both channels driven by the spike protocol (dashed line). Under this more biologically realistic protocol, the roles are reversed. Now, the Na^+ dissipates significantly more than the K^+ channel and does so responding much more rapidly to changes in membrane voltage. This suggests a tradeoff between the speed of the channel's response and its dissipation, one not necessarily present in the more artificial pulse protocol.

of the protocol, but *also* appears to respond much more quickly to changes in the protocol than does the K^+ channel. A tradeoff appears: the cost of the Na^+ channel adapting more *quickly* to its environment is that it dissipates more in the process. This did not arise when driven by the pulse protocol. (Likely, this is due to that protocol operating outside of the "normal" voltage range for these channels—by dropping as low as -100 mV.)

Besides showcasing a detailed energetic comparison between different channels, the discrepancy between the pulse- and spike-driven behaviors demonstrate that *in vivo* thermodynamic response can qualitatively differ

from that elicited by voltage-clamp experiments.

The corresponding results for excess work are given in Figs. 9 and 10. Unlike excess heat, the excess work is not sensitive to the timescales of each channel's relaxation to steady state. Instead, it tracks *environmental* entropy produced by the external drive. Yet it is still sensitive to the dynamics of the individual model (per Eq. (8)), and this sensitivity is reflected in the thermodynamic responses.

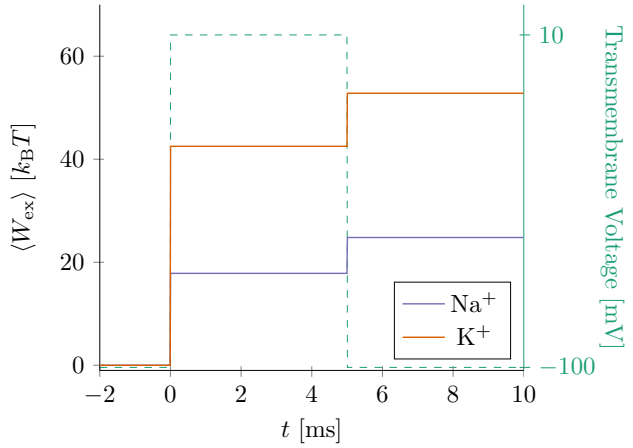

FIG. 9. Excess works (solid lines) for both channels under the pulse protocol (dashed line). Unlike excess heat, excess work is only done upon *change* in the driving parameter. Thus, we see changes only at the pulse's rise and fall. Much more excess work is done on the K^+ channel than on the Na^+ during the rise. More is done on the Na^+ channel during the fall, but not enough to make up for the initial discrepancy.

As in the excess heat calculations, there is a discrepancy in behavior between the pulse and spike protocols. In the former, the K^+ channel induces much larger *total* excess work under the same protocol, but it is entirely due to the initial jump from -100 to 10 mV. The drop, from 100 back to -10 mV, sees the Na^+ channel inducing more excess work.

Driven by the spike protocol, the Na^+ channel induces significantly more environmental entropy production across the board. This reflects the larger potential for dissipation in the Na^+ channel under the spike protocol, as seen in the case of excess heat.

To reiterate, while excess heat is an energetic signature of relaxation to steady state, these calculations do not assume the system ever *reaches* such a steady state. While the pulse protocol allows each of the channels to do so, over the course of the spike we see a *dynamic* dissipation in the two channels—this is energy expended while attempting to reach an ever-evolving steady-state target. We close by highlighting that our theoretical developments enabled quantitatively comparing the channels' adaptive energetics under realistic environmental stimuli—captured in our Fig. 8—*despite* the departures in their underlying steady-state dissipation.

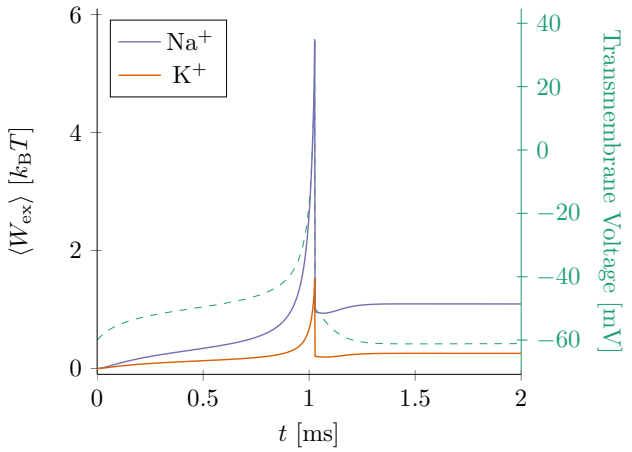

FIG. 10. Excess works (solid lines) for both channels under the spike protocol (dashed line). We see that more excess work is done on the Na^+ channel across the board. This corresponds to larger environmental entropy production and indicates a greater potential for dissipated work in the Na^+ channel.

VI. CONCLUSION

We reviewed and extended the techniques of stochastic thermodynamics, culminating in a trajectory class fluctuation theorem for nonequilibrium steady-states and, even, for nonthermal stochastic processes. Using these, we analyzed the adaptive and homeostatic energetic signatures of two neurobiological systems—systems key to propagating action potentials in mammalian neurons. Along the way, we developed a toolkit for probing the nonequilibrium thermodynamics in a broad range of mesoscopic complex systems that requires little in the way of restrictive assumptions.

Our results exposed a new quantitative structure in how systems appear to violate equilibrium steady-state assumptions, both warning against and elucidating the consequences of inappropriately assuming detailed balanced dynamics. In this, they suggest a need for new experimental tools. Superficially, for nonequilibrium steady-state systems, tracking housekeeping entropy production is *crucial* to extracting functionally relevant thermodynamics.

Finally, the spike protocol simulations of average excess energetics also identified what *would not* be observed in traditional patch-clamp experiments on ion channels. Under the more dynamical (and realistic) protocol, the Na^+ channel dissipates significantly more than the K^+ channel, but the roles are reversed in the pulse protocol that more accurately simulates a fixed-voltage patch-clamp design.

Taken together, our development and associated numerical experiments revealed a rich—and, indeed, necessary—set of tools with which to probe the nonequilibrium dynamics of mesoscopic complex systems.

ACKNOWLEDGMENTS

The authors thank Paul Riechers, Gregory Wimsatt, Samuel Loomis, Alex Jurgens, Alec Boyd, Kyle Ray, Adam Rupe, Ariadna Venegas-Li, David Geier, and Adam Kunesh for helpful discussions; as well as the Telluride Science Research Center for hospitality during visits and the participants of the Information Engines Workshops there for their feedback and discussion. This material is based upon work supported by, or in part by, FQXi Grant number FQXi-RFP-IPW-1902, and U.S. Army Research Laboratory and the U.S. Army Research Office under grants W911NF-18-1-0028 and W911NF-21-1-0048.

Appendix A: NESS TCFT Derivation

In addition to the requiring a unique stationary distribution for each protocol value, we assume that for any $x_{0:N} \in \mathcal{X}^{N+1}$:

- $x_{N:0} \in \mathcal{X}^{N+1}$,
- $\mathcal{P}_{\boldsymbol{\mu}_\mathrm{F}}(x_{0:N}) \neq 0 \implies \mathcal{P}_{\boldsymbol{\mu}_\mathrm{F}}(x_{N:0}) \neq 0$, and
- $\mathcal{R}_{\boldsymbol{\mu}_\mathrm{R}}(x_{N:0}) \neq 0 \implies \mathcal{R}_{\boldsymbol{\mu}_\mathrm{R}}(x_{0:N}) \neq 0$.

The second and third requirements, in particular, forbid one-way-only transitions in the discrete-time dynamic. Once we derive the TCFT, we will discuss the edge cases of completely irreversible trajectories.

Given the preceding constraints, a slightly rearranged form of Ref. [13]'s NESS DFT reads:

$$\mathcal{R}_{\boldsymbol{\mu}_\mathrm{R}}(x_{N:0}) = \mathcal{P}_{\boldsymbol{\mu}_\mathrm{F}}(x_{0:N})\, \mathrm{e}^{-(\mathcal{W}_\mathrm{ex} + \mathcal{Q}_\mathrm{hk} - \Delta\mathcal{F}^\mathrm{nss})} \ .$$

We wish to integrate both sides over a *trajectory class*—the measurable subset $C \subseteq \mathcal{X}^{N+1}$ of trajectories. We also define the *reverse trajectory class* $C_\mathrm{R} \doteq \{\, x_{N:0} \,|\, x_{0:N} \in C \,\}$. The following derivation mimics that of Ref. [33] after their Eq. (F3).

Integrating the lefthand side gives:

$$\begin{aligned}
\int [x_{0:N} \in C]\, \mathcal{R}_{\boldsymbol{\mu}_\mathrm{R}}(x_{N:0})\, \mathrm{d}x_{0:N} & \\
&= \int [x_{0:N} \in C]\, \mathcal{R}_{\boldsymbol{\mu}_\mathrm{R}}(x_{N:0})\, \mathrm{d}x_{N:0} \\
&= \int [x_{N:0} \in C_\mathrm{R}]\, \mathcal{R}_{\boldsymbol{\mu}_\mathrm{R}}(x_{N:0})\, \mathrm{d}x_{N:0} \\
&= \mathcal{R}_{\boldsymbol{\mu}_\mathrm{R}}(C_\mathrm{R}) \ ,
\end{aligned}$$

where $[\cdot]$ is the Iverson bracket.
Integrating the righthand side gives:

$$\begin{aligned}
\int [x_{0:N} \in C]\, \mathcal{P}_{\boldsymbol{\mu}_\mathrm{F}}(x_{0:N})\, \mathrm{e}^{-(\mathcal{W}_\mathrm{ex} + \mathcal{Q}_\mathrm{hk} - \Delta\mathcal{F}^\mathrm{nss})}\, \mathrm{d}x_{0:N} & \\
&= \int \mathcal{P}_{\boldsymbol{\mu}_\mathrm{F}}(x_{0:N} \cap C)\, \mathrm{e}^{-(\mathcal{W}_\mathrm{ex} + \mathcal{Q}_\mathrm{hk} - \Delta\mathcal{F}^\mathrm{nss})}\, \mathrm{d}x_{0:N} \\
&= \mathcal{P}_{\boldsymbol{\mu}_\mathrm{F}}(C) \times \\
&\qquad \int \mathcal{P}_{\boldsymbol{\mu}_\mathrm{F}}\left(x_{0:N} \,|\, C\right)\, \mathrm{e}^{-(\mathcal{W}_\mathrm{ex} + \mathcal{Q}_\mathrm{hk} - \Delta\mathcal{F}^\mathrm{nss})}\, \mathrm{d}x_{0:N} \\
&= \mathcal{P}_{\boldsymbol{\mu}_\mathrm{F}}(C) \left\langle \mathrm{e}^{-(\mathcal{W}_\mathrm{ex} + \mathcal{Q}_\mathrm{hk} - \Delta\mathcal{F}^\mathrm{nss})} \right\rangle_C \ ,
\end{aligned}$$

where $\langle \cdot \rangle_C$ is the average over the trajectory class C. Thus, we have Eq. (18)—a TCFT for NESS systems, whose forward and reverse processes may start in arbitrary distributions:

$$\frac{\mathcal{R}_{\boldsymbol{\mu}_\mathrm{R}}(C_\mathrm{R})}{\mathcal{P}_{\boldsymbol{\mu}_\mathrm{F}}(C)} = \left\langle \mathrm{e}^{-(\mathcal{W}_\mathrm{ex} + \mathcal{Q}_\mathrm{hk} - \Delta\mathcal{F}^\mathrm{nss})} \right\rangle_C . \tag{A1}$$

Now, it remains to investigate the edge cases. Suppose that either (i) $\mathcal{P}_{\boldsymbol{\mu}_\mathrm{F}}(C) = 0$ or (ii) $\mathcal{R}_{\boldsymbol{\mu}_\mathrm{R}}(C_\mathrm{R}) = 0$, but not both (which would amount to analyzing fluctuations for a *pair* of trajectories which never occur). Since our probabilities are strictly nonnegative, the possible behaviors of the left hand side are either $+\infty$ or 0, respectively, by considering the limit of a vanishing probability. In case (i), by definition either $\mathrm{e}^{-\mathcal{Q}_\mathrm{hk}} \to +\infty$ or $\mathrm{e}^{\Delta\mathcal{F}^\mathrm{nss}} \to +\infty$ (or both) for each forward trajectory, yielding agreement with the left hand side. In case (ii), similarly either $\mathrm{e}^{-\mathcal{Q}_\mathrm{hk}} \to 0$ or $\mathrm{e}^{\Delta\mathcal{F}^\mathrm{nss}} \to 0$ (or both) for each forward trajectory. Since the preceding derivation established the TCFT for all non-diverging cases, this establishes its truth even in the divergent limiting cases.

[1] M. C. Cross and P. C. Hohenberg. Pattern formation outside of equilibrium. *Rev. Mod. Phys.*, 65(3):851–1112, 1993.

[2] E. H. Trepagnier, C. Jarzynski, F. Ritort, G. E. Crooks, C. J. Bustamante, and J. Liphardt. Experimental test of Hatano and Sasa's nonequilibrium steady-state equality. *Proc. Natl. Acad. Sci. U.S.A.*, 101(42):15038–15041, 2004.

[3] M. Esposito. Stochastic thermodynamics under coarse graining. *Phys. Rev. E*, 85(4):041125, 2012.

[4] C. Y. Gao and D. T. Limmer. Principles of low dissipation computing from a stochastic circuit model. *arXiv:2102.13067*, 2021.

[5] Y. Oono and M. Paniconi. Steady State Thermodynamics. *Prog. Theor. Phys. Suppl.*, 130:29–44, 1998.

[6] With important exceptions, particularly in the first sense, under small perturbations from equilibrium [40, 41].

[7] C. Jarzynski. Equilibrium free-energy differences from nonequilibrium measurements: A master-equation approach. *Phys. Rev. E*, 56(5):5018–5035, 1997.

[8] C. Jarzynski. Nonequilibrium Equality for Free Energy Differences. *Phys. Rev. Lett.*, 78(14):2690–2693, 1997.

[9] G. E. Crooks. Entropy production fluctuation theorem and the nonequilibrium work relation for free energy differences. *Phys. Rev. E*, 60(3):2721–2726, 1999.

[10] G. E. Crooks. Nonequilibrium Measurements of Free Energy Differences for Microscopically Reversible Markovian Systems. *J. Stat. Phys.*, 90(5-6):1481–1487, 1998.

[11] T. Hatano and S.-i. Sasa. Steady-State Thermodynamics of Langevin Systems. *Phys. Rev. Lett.*, 86(16):3463–3466, 2001.

[12] T. Speck and U. Seifert. Integral fluctuation theorem for the housekeeping heat. *J. Phys. A: Math. Gen.*, 38(34):L581–L588, 2005.

[13] P. M. Riechers and J. P. Crutchfield. Fluctuations When Driving Between Nonequilibrium Steady States. *J. Stat. Phys.*, 168(4):873–918, 2017.

[14] U. Seifert. Stochastic thermodynamics: From principles to the cost of precision. *Physica A*, 504:176–191, 2018.

[15] P. Dayan and L. F. Abbott. *Theoretical Neuroscience: Computational and Mathematical Modeling of Neural Systems*. Computational Neuroscience. Massachusetts Institute of Technology Press, Cambridge, Mass, 2001.

[16] J. Schnakenberg. Network theory of microscopic and macroscopic behavior of master equation systems. *Rev. Mod. Phys.*, 48(4):571–585, 1976.

[17] T. M. Cover and J. A. Thomas. *Elements of Information Theory*. Wiley-Interscience, second edition, 2006.

[18] J. P. Sethna. *Entropy, Order Parameters, and Complexity*. Oxford Master Series in Physics. Oxford University Press, Oxford, second edition, 2021.

[19] R. E. Spinney and I. J. Ford. Nonequilibrium Thermodynamics of Stochastic Systems with Odd and Even Variables. *Phys. Rev. Lett.*, 108(17):170603, 2012.

[20] J. Yeo, C. Kwon, H. K. Lee, and H. Park. Housekeeping entropy in continuous stochastic dynamics with odd-parity variables. *J. Stat. Mech.*, 2016(9):093205, 2016.

[21] R. J. Harris and G. M. Schütz. Fluctuation theorems for stochastic dynamics. *J. Stat. Mech.*, 2007(07):P07020–P07020, 2007.

[22] G. Wimsatt, O.-P. Saira, A. B. Boyd, M. H. Matheny, S. Han, M. L. Roukes, and J. P. Crutchfield. Harnessing fluctuations in thermodynamic computing via time-reversal symmetries. *Phys. Rev. Res.*, 3(3):033115, 2021.

[23] U. Çetiner, O. Raz, S. Sukharev, and C. Jarzynski. Recovery of Equilibrium Free Energy from Nonequilibrium Thermodynamics with Mechanosensitive Ion Channels in *E. coli*. *Phys. Rev. Lett.*, 124(22):228101, 2020.

[24] C. Jarzynski. Rare events and the convergence of exponentially averaged work values. *Phys. Rev. E*, 73(4):046105, 2006.

[25] G. Hummer and A. Szabo. Free energy reconstruction from nonequilibrium single-molecule pulling experiments. *Proc. Natl. Acad. Sci. U.S.A.*, 98(7):3658–3661, 2001.

[26] J. Liphardt, S. Dumont, S. B. Smith, I. Tinoco, and C. Bustamante. Equilibrium Information from Nonequilibrium Measurements in an Experimental Test of Jarzynski's Equality. *Science*, 296(5574):1832–1835, 2002.

[27] C. Jarzynski. Work Fluctuation Theorems and Single-Molecule Biophysics. *Prog. Theor. Phys. Suppl.*, 165:1–17, 2006.

[28] U. Seifert. Stochastic thermodynamics, fluctuation theorems and molecular machines. *Rep. Prog. Phys.*, 75(12):126001, 2012.

[29] D. Collin, F. Ritort, C. Jarzynski, S. B. Smith, I. Tinoco, and C. Bustamante. Verification of the Crooks fluctuation theorem and recovery of RNA folding free energies. *Nature*, 437(7056):231–234, 2005.

[30] S. Lahiri and A. M. Jayannavar. Fluctuation theorems for excess and housekeeping heat for underdamped Langevin systems. *Eur. Phys. J. B*, 87(9):195, 2014.

[31] D. Mandal, K. Klymko, and M. R. DeWeese. Entropy Production and Fluctuation Theorems for Active Matter. *Phys. Rev. Lett.*, 119(25):258001, 2017.

[32] C. A. Vandenberg and F. Bezanilla. A sodium channel gating model based on single channel, macroscopic ionic, and gating currents in the squid giant axon. *Biophys. J.*, 60(6):1511–1533, 1991.

[33] G. Wimsatt, O.-P. Saira, A. B. Boyd, M. H. Matheny, S. Han, M. L. Roukes, and J. P. Crutchfield. Harnessing fluctuations in thermodynamic computing via time-reversal symmetries. *Phys. Rev. Research*, 3(3):033115, 2021.

[34] O.-P. Saira, M. H. Matheny, R. Katti, W. Fon, G. Wimsatt, J. P. Crutchfield, S. Han, and M. L. Roukes. Nonequilibrium thermodynamics of erasure with superconducting flux logic. *Phys. Rev. Research*, 2(1):013249, 2020.

[35] A. L. Hodgkin and A. F. Huxley. A quantitative description of membrane current and its application to conduction and excitation in nerve. *J. Physiol.*, 117(4):500–544, 1952.

[36] K. Pal and G. Gangopadhyay. Dynamical characterization of inactivation path in voltage-gated Na$\hat{}\{+\}$ ion channel by non-equilibrium response spectroscopy. *Channels*, 10(6):478–497, 2016.

[37] E. Marban, T. Yamagishi, and G. F. Tomaselli. Structure and function of voltage-gated sodium channels. *J. Physiol.*, 508(3):647–657, 1998.

[38] E. M. Izhikevich. *Dynamical Systems in Neuroscience: The Geometry of Excitability and Bursting*. Computational Neuroscience. The MIT Press, first edition, 2006.

[39] E. M. Izhikevich. Simple model of spiking neurons. *IEEE Trans. Neural Netw.*, 14(6):1569–1572, 2003.

[40] L. Onsager. Reciprocal relations in irreversible processes, I". *Phys. Rev.*, 37(4):405–426, 1931.

[41] D. Kondepudi. *Introduction to Modern Thermodynamics*. Wiley, Chichester, 2008.